A&A 376, 553–560 (2001)
DOI: 10.1051/0004-6361:20010979

Astronomy & Astrophysics

Multiple H_2 protostellar jets in the bright-rimmed globule IC 1396-N⋆

B. Nisini[1], F. Massi[2], F. Vitali[1], T. Giannini[1], D. Lorenzetti[1], A. Di Paola[1], C. Codella[3], F. D'Alessio[1], and R. Speziali[1]

[1] Osservatorio Astronomico di Roma, 00040 Monteporzio Catone, Italy
[2] Osservatorio Astronomico di Collurania-Teramo, Via M. Maggini, 64100 Teramo, Italy
[3] CNR-Istituto di Fisica dello Spazio Interplanetario, Area di Ricerca Tor Vergata, Via Fosso del Cavaliere 100, 00133 Roma, Italy

Received 13 March 2001 / Accepted 5 July 2001

Abstract. We present near infrared images of the bright rimmed globule IC 1396-N in the H_2 2.12 μm narrow band filter as well as in broad band J, H and K filters. We detected several chains of collimated H_2 knots inside the globule, having different luminosities but similar orientations in the sky. Most of the knots are associated with peaks of high velocity CO emission, indicating that they trace shocked regions along collimated stellar jets. From the H_2 knots morphology and orientation, we identify at least three different jets: one of them is driven by the young protostar associated with IRAS 21391+5802, which represents the most luminous object in the region, while we were able to identify only one of the two other driving sources by means of near infrared photometry. Our photometry reveals the existence of a cluster of young embedded sources located in a south-north line which follows the distribution of the high density gas and testifies for a highly efficient star formation activity through all the globule.

Key words. stars: formation – ISM: jets and outflows – ISM: individual objects: IC 1396-N – infrared: ISM: lines

1. Introduction

IC 1396 is an extended H II region located in the Cep OB2 association (at a distance of 750 pc) and excited by the O6 star HD 206267. Inside the ionised region, several globules have been identified, characterised by their optically visible bright rim tracing the ionisation front in the direction of the O6 star (Osterbrock 1957). Such globules have long been suspected to be sites of star formation induced by the compression due to the ionisation shock front. The association of some of these globules with IRAS sources has given further support to this hypothesis (Sugitani et al. 1991). IC 1396-N, located at about 11 pc of projected distance from HD 206267, is associated with the brightest of these IRAS sources (21391+5802, $L_{\rm bol} \sim 300\ L_{\odot}$, e.g. Wilking et al. 1993) showing a very cold far infrared spectrum and a large circumstellar mass (Wilking et al. 1993; Sugitani et al. 2000), indicating that it should be in an early stage of evolution. Furthermore this source drives an energetic outflow having a dynamical time $<10^5$ yr (Sugitani et al. 1989; Codella et al. 2001). These findings represent strong evidence for an on-going star formation activity triggered by radiation-driven implosion, although evidences for a spontaneous onset of the collapse are also provided (Serabyn et al. 1993).

IC 1396-N has been recently also observed with the ISO spectrometers. The far-infrared spectrum from the environments of the IRAS source is extremely rich of molecular emission excited at a temperature in excess of 1500 K (Saraceno et al. 1996) in a dense shock originated along the protostellar outflow. Such a high temperature is expected to give rise also to copious emission from the rotovibrational transitions of H_2 and in particular from the 1–0 S(1) line at 2.12 μm. In this paper we report the results of narrow band imaging in this line covering all the IC 1396-N globule. These observations provide a powerful tool both to study the morphology of the shocked gas and to indirectly reveal the presence of young embedded sources inside the globule. The narrow band images are also complemented with J, H and K photometry of the region, allowing to study the young star population and test the hypothesis of the triggered star formation.

Send offprint requests to: B. Nisini,
e-mail: bruni@coma.mporzio.astro.it

⋆ Based on observations collected with the AZT-24 Telescope at Campo Imperatore, a joint project between the Astronomical Observatories of Roma (OAR, Italy), Teramo (OACT, Italy) and Pulkovo (OAP, Russia).

2. Observations and results

The observations were carried out on several nights in 1999 and 2000 using the 256×256 PICNIC near-infrared camera SWIRCAM (D'Alessio et al. 2000), on the 1.1-m telescope AZT-24 located at Campo Imperatore (Italy). The scale is 1.″04/pixel which gives a total FOV of about 4.′4 × 4.′4.

The IC 1396-N globule has been mapped in the narrow-band ($\Delta\lambda = 0.021$ μm) filter centred on the H_2 1−0 S(1) line ($\lambda = 2.122$ μm). In addition, broad-band JHK images of a field centred on the IRAS source position ($\alpha_{1950} = 21^h39^m10.3^s, \delta_{1950} = +58°02'29''$) have been obtained.

The narrow-band H_2 images were obtained on August 19 and September 30, 1999 along with images of the standard star HD 203856 (Elias et al. 1982). The total integration time in the narrow band filter was 40 min per image. J, H and K images were acquired on August 18, 1999, September 30, 1999 and August 30, 2000. The integration times for these images were 11 min in the K band and 5 min in the J and H bands, allowing sensitivity limits (at 3σ) of $J = 18.4$, $H = 17.6$ and $K = 16.3$ mag. We estimated a completeness limit of 15 mag in the K band. Flux calibration of the continuum images was made by means of observations of the IR standard stars AS35, AS 37-1 and AS37-0 (Hunt et al. 1998). Differential flat-field frames were obtained through images of the illuminated dome or the sky at setting. Data reduction was performed using IRAF routines and included flat-field correction and subtraction of a sky frame constructed by combining different on-sky images through a median filtering. Photometry on the observed fields was performed through PSF-fitting using DAOPHOT in IRAF. Aperture corrections were estimated by accurately studying the growth curves both of bright isolated field stars and of the standard stars themselves. Seeing ranged from ∼2 to ∼3 arcsec, whereas zero point variations of ∼0.1 mag were found in the photometry of the standard stars before and after the field observations. These are of the same order of the zero point variations found in a same frame when more than 1 standard star are imaged.

The astrometric calibration was obtained by using stars recognisable both in our frames and in the Palomar Digitized Sky Survey (DSS). The resulting accuracy is within 1 arcsec. Figure 1 shows the region covered by our mosaic on a $10' \times 10'$ DSS image; the bright rim underlining the dark globule is clearly visible. Figure 2 shows the K image of the central region of the globule; a number of infrared sources are located inside the optically dark region, together with patches of nebulosity and extended emission. The source IRAS 21391+5802 is marked with a cross and its uncertainty ellipse is also overlaid. The bright rim structure is still visible also at 2 μm.

Figure 3 shows the H_2 2.12 μm plus continuum emission in the investigated field. The figure is a mosaic of three different images (see Fig. 1), covering a total area of about 44 arcmin^2.

An image of the pure H_2 emission has been constructed by subtracting the broad-band K image to the narrow-band image after having corrected for the different integration times and filters characteristics.

Figure 4 shows the result of this subtraction in the region of the mosaic where the H_2 emission has been detected. The position of IRAS 21391+5802 is marked with an asterisk. Several jets of H_2 emission are present all over the image and seem to trace different flows; we have labelled the most prominent emission knots from A to G giving their position and luminosity in Table 1.

Table 1. Positions and 2.12 μm luminosity of the H_2 knots.

	α (1950)	δ (1950)	$L_{2.12\mu m}/L_\odot$	$L_{tot}/L^a_\odot$
A	21:39:12	58:02:38	0.025	2.3
B	21:39:24	58:02:59	0.026	0.73
C	21:39:03	58:04:40	0.036	1.0
F	21:39:10	58:04:58	0.008	0.22
E	21:39:04	58:03:58	0.005	0.14
D	21:39:14	58:04:02	0.006	0.17
G	21:39:06	58:03:17	0.004	0.11

[a] Total H_2 luminosity estimated as $L_{tot} = 10 \times L_{2.12\mu m} \times 10^{A_k/2.5}$, where $A_k = 0.112\ A_v$ and A_v is taken equal to 20 mag for knot A and 10 mag elsewhere (see Sect. 3.2).

3. Discussion

3.1. Morphology and excitation of the H_2 emission

In principle, H_2 excitation inside the globule could be due either to shocks driven by the outflows of young stellar objects or to fluorescence induced by the UV photons from the external ionised region. The jet-like morphology of the H_2 emission knots and their location in different parts of the globule and not just on the bright rim, can be considered an indication more in favour of shocked gas along stellar jets. A more quantitative analysis to establish how much of the observed emission could be attributed to fluorescent excitation can be done by estimating the FUV field associated with the ionising front. The far infrared spectra obtained by ISO-LWS (with a FOV of about 80″) provide a measure of the [C II] 158 μm line brightness of $\sim 1.2 \times 10^{-4}$ erg s^{-1} cm^{-2} sr^{-1}, almost constant in three different positions of the globule (Saraceno, private communication). This value translates into a FUV flux of ∼120 G_0, where $G_0 = 1.6 \times 10^{-3}$ erg s^{-1} cm^{-2} is a measure of the average local interstellar field (Habing 1968), adopting the relationship $I_{158\mu m} = 10^{-6}\ G_0$ erg s^{-1} cm^{-2} sr^{-1} (Hollenbach et al. 1991). The H_2 2.12 μm intensity produced by fluorescence in a photo-dissociation region with this field is expected to be lower than 10^{-5} erg s^{-1} cm^{-2} sr^{-1} for densities $<10^6$ cm^{-3} (e.g. Burton et al. 1992).

The observed knots show H_2 intensities between 10 and 100 times larger than this value, thus excluding

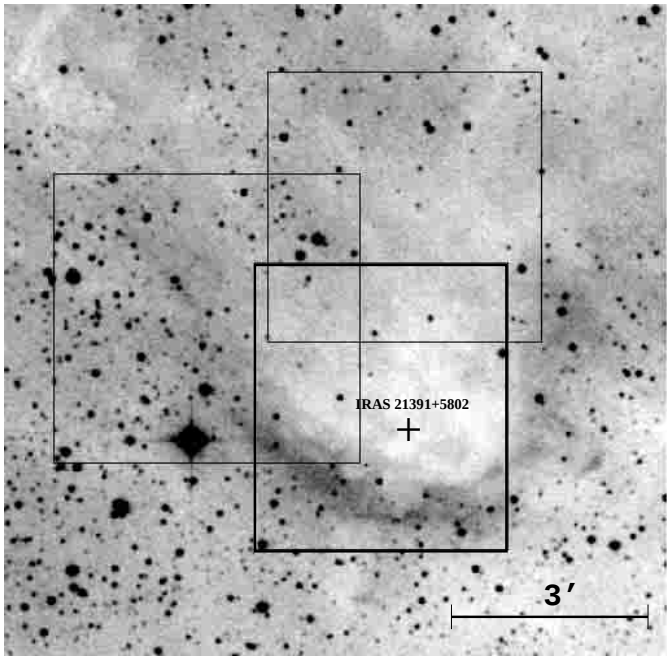

Fig. 1. $10' \times 10'$ Palomar map of the IC 1396-N globule. The squares indicate the regions covered by our observations while the cross marks the position of the IRAS source with coordinates $\alpha_{1950} = 21^h39^m10.3^s, \delta_{1950} = +58°02'29''$.

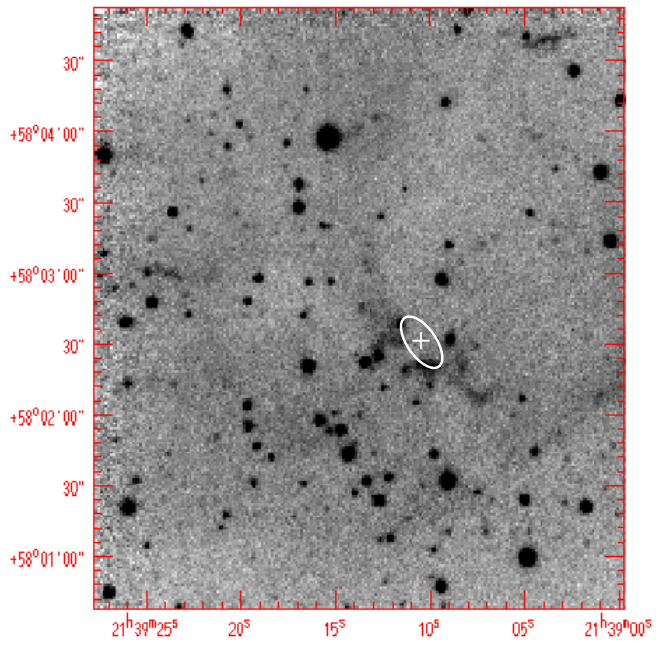

Fig. 2. K image of the central region of the globule (corresponding to the thickest frame in Fig. 1). The cross indicates the position of the IRAS source for which also the uncertainty ellipse is delineated. Right ascension and declination are at 1950.

fluorescent emission as the main mechanism for their excitation. On the other hand, non-dissociative shocks with velocities larger than ∼20 km s^{-1} can easily produce the observed strength of the 2.12 μm line. In order to better clarify this interpretation, we have compared our H_2 image with a map of the high velocity CO $J = 2-1$ emission taken from Codella et al. (2001). Figure 5 shows the two maps superimposed each other; the solid and dashed contours refer to the blue- and the red-shifted gas respectively. As discussed in Codella et al., the CO emission detected in the globule clearly presents a double component; a low velocity gas delineating the globule structure and probably put into motion by the action of the external radiation field, and high velocity, (up to 40 km s^{-1}), bipolar components which are clearly associated with outflowing gas from young stellar objects. Most of the H_2 knots are associated with these high velocity CO peaks, thus reinforcing the interpretation of shock excitation.

From this figure it clearly appears that the two clumps A and B are associated with the more extended outflow emanating from the IRAS source, which was originally discovered by Sugitani et al. (1989) (here called outflow I). The H_2 knot A is close to the IRAS position and associated with both a blue and a red CO peak. Knot B is located towards a second CO peak of blueshifted emission, which is extended eastward. The red part of the flow is less extended and collimated; here the outflow seems to bend towards north as it interacts with the wall of the globule. No H_2 emission is observed from this red lobe, due either to a higher extinction (a value of $A_v \sim 35$ mag would be required in order not to detect H_2 emission of the same strength as the blue lobe), or to a much lower pre-shock density encountered by the flow, producing a weaker shock interaction.

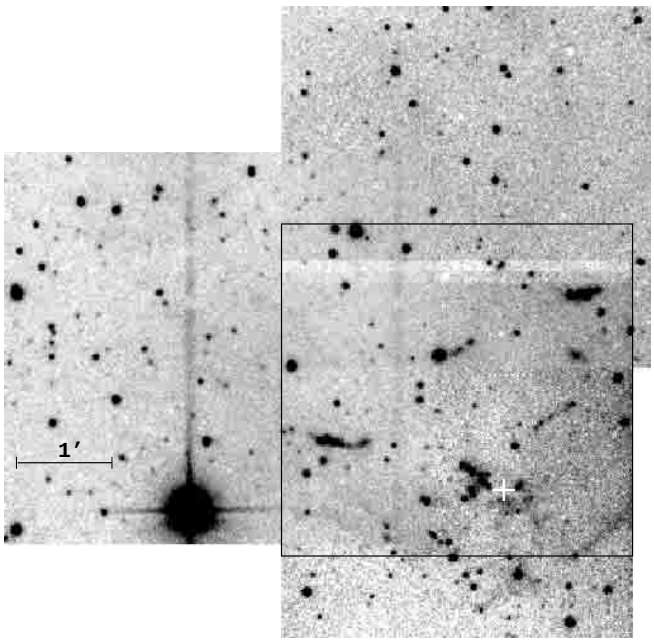

Fig. 3. H_2 2.12 μm + continuum image of the observed region. The rectangle delimits the core of the IC 1396-N globule from which pure H_2 emission in the form of several clumps has been detected (see Fig. 4).

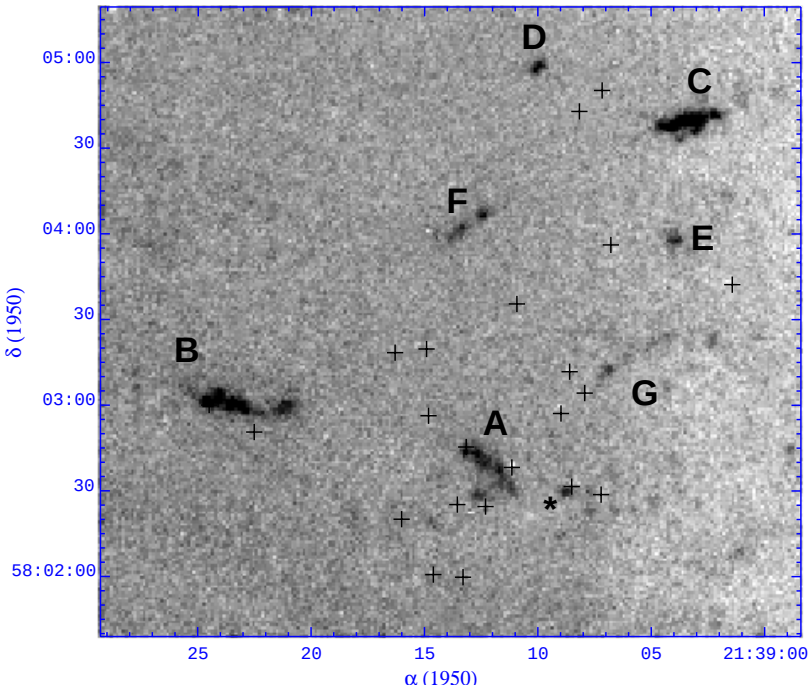

Fig. 4. Continuum subtracted H_2 2.12 μm image of the central region of IC 1396-N ($\sim 4'.4 \times 4'.4$). The most prominent clumps of emission have been labelled from A to G. The asterisk indicates the position of the IRAS source, while the crosses mark the position of young embedded sources identified through the near IR photometry (see Sect. 3.4).

Two additional outflows can be tentatively identified from the comparison of the CO and the H_2 maps. Considering only the H_2 knots morphology and alignments, one would be tempted to assume that knots C and F belong to the blue and red-shifted parts of the same outflow, in which case knots D and E would define a third outflow aligned perpendicularly to it. However, a 1.3 millimeter continuum map of this northern region of the globule (Codella et al. 2001), reveals a peak of emission just at the center of the axis connecting knots D and C, suggesting the presence of a cold source which could excite these shock condensations. Therefore D and C are probably associated with the two lobes of the same flow (outflow III) while an additional flow (outflow II) could be associated with knots F and E. These two outflows present a more compact structure and a weaker CO emission with respect to outflow I. Knot C has an H_2 intensity comparable to knots A and B (see Table 1), while the intensity of knot D can be weaker due to its association with red-shifted gas and thus with larger extinction regions. On the other hand, knots E and F are both fainter than the other clumps, indicating presumably a weaker shock interaction (see also next section). Finally, the knot labelled as G in the H_2 image cannot be easily associated with any of the CO peaks although it is clearly located in a region of enhanced high-velocity CO emission.

It is remarkable that all the three identified jets are oriented with a position angle of about 80° with respect to the North. This preferred orientation strongly resemble the orientation shown by the magnetic field lines on the border of externally illuminated globules as observed by Hodapp (1987). The explanation given for such orientation is that in the outer parts of the globule the magnetic field is aligned by the wind or radiation effects coming from the centre of the HII region; the outflows will be then aligned with the magnetic field direction.

3.2. Shock properties

The good spatial coincidence of the H_2 knots with the peaks of high-velocity CO integrated emission gives support to the idea that the observed H_2 emission originates in the shocks occurring at the head of a collimated stellar jet when it interacts with the ambient molecular gas; in this scenario the shock causes the ambient gas to be swept up at large distances from the jet itself (Masson & Chernin 1993; Raga & Cabrit 1993).

From Table 1 we can have an estimate of the total H_2 energy radiated away by each of the detected shock events, assuming that the S(1) line represents about 1/10 of the radiation emitted by H_2 in all the rotovibrational lines; this is a valid approximation for a thermalised gas at about 2000 K. The so found total luminosity needs to be corrected for the 2.12 μm extinction which can be severe especially for the knot A which is located close to the highly embedded IRAS source. Indeed, from millimeter maps of the central region of IC 1396-N, visual extinction values as high as $A_V > 60$ mag can be inferred in the direction of the exciting source (Wilking et al. 1993; Sugitani et al. 2000). Knot A is at about 20″ away from the millimeter peak and it is expanding in a direction of decreasing column density. If we scale the clump column density according to the density profile derived by Serabyn et al. (1993), we can infer a visual extinction of about 20 mag in the direction of knot A. Assuming this visual extinction, the intrinsic total H_2 luminosity becomes 2.3 $L_\odot$.

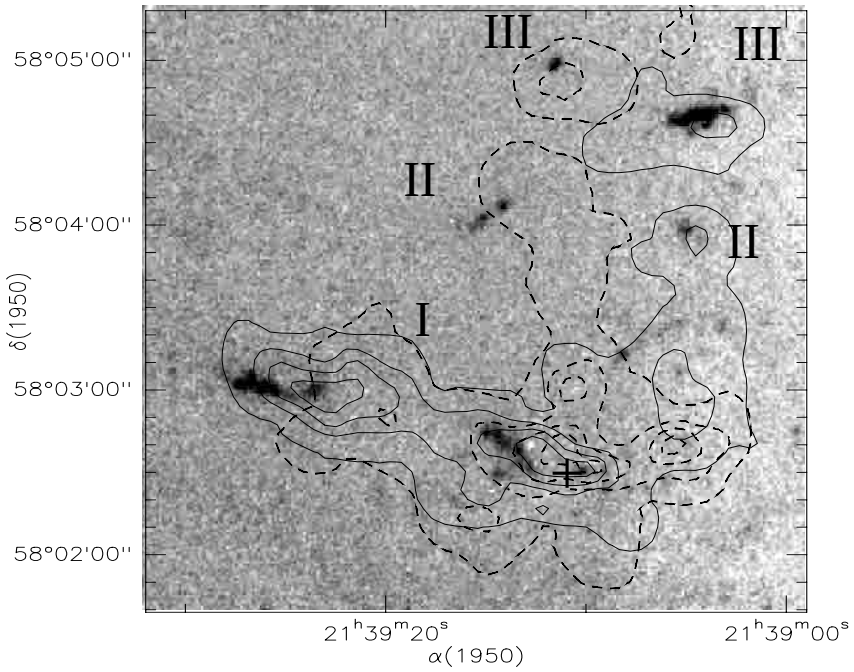

Fig. 5. Continuum subtracted H_2 2.12 μm image with superimposed the CO $J = 2 - 1$ map of high velocity gas from Codella et al. (2001). The solid and dashed contours show the blue- and the red- shifted gas respectively. The contours refer to the emission integrated in the velocity interval |6–9| km s^{-1}. The three flows associated with the observed H_2 emission are indicated with roman numbers. The cross indicates the IRAS source position.

For knot B, as well as for the other H_2 emission knots, we assume a lower extinction value of 10 mag, which is the average extinction derived from the color-color diagram shown in Fig. 6 by looking at the location of the sources having reddened main sequence colors. In Table 1, the so derived intrinsic luminosities are reported for each knot.

In addition to H_2, a significant contribution to the cooling of the post shocked gas is expected from other molecules and atoms, such as O I, CO and H_2O (i.e. Kaufman & Neufeld 1996). Indeed, the observations carried out by the Infrared Space Observatory towards IRAS 21391+5802 have detected strong emission from these species whose total cooling amount to about 0.9 $L_\odot$ (Saraceno et al. 1996; Nisini et al. 1998). This represents one third of the H_2 luminosity derived here for clump A, which is also encompassed by the ISO spectrometer field of view. We can assume that the same ratio also applies for the other observed knots of shocked emission. In this way, we can have an estimate of the total cooling in the post-shocked gas ($L_{\rm rad}$), which, if the shock is fully radiative, can be expressed as:

$$L_{\rm rad} = \frac{1}{2} v_{\rm s}^3 \cdot \rho_{\rm o} \cdot A_{\rm eff}, \quad (1)$$

where $v_{\rm s}$ is the shock velocity, $\rho_{\rm o}$ is the pre-shock density and $A_{\rm eff}$ is the effective area of the shock front. This expression can be more conveniently written as:

$$L_{\rm rad} = 3.5 \times 10^4 \cdot \left(\frac{v_{\rm s}}{100\,{\rm km\,s^{-1}}}\right)^3 \cdot \left(\frac{n_{\rm o}}{10^5\,{\rm cm^{-3}}}\right) \cdot \left(\frac{\Omega}{\rm sr}\right) L_\odot \cdot \quad (2)$$

With the derived total shock luminosity and assuming a pre-shock density, we are able from (2) to estimate the shock velocity for the H_2 knots which are associated with the CO peaks. From the cloud gas density profile derived by Serabyn et al. (1993), we assume an ambient density of $\sim 10^5\,{\rm cm^{-3}}$ towards knot A, and $\sim 3 \times 10^4\,{\rm cm^{-3}}$ towards the other knots. The application of Eq. (2) with these density values gives $v_{\rm s} \simeq 36$ km s^{-1} for knots A and B, $v_{\rm s} \simeq 30$ km s^{-1} for C and $v_{\rm s} \simeq 24$ km s^{-1} for E. Such values are in the range of velocities expected to give rise to non-dissociative C-shocks in which the H_2 emission represents the main cooling channel.

If we consider the entire outflow I, its total shock radiated luminosity $L_{\rm rad} = L_{\rm H_2} + L_{\rm FIR}$ is about 4 $L_\odot$. This value is much higher than the $L_{\rm kin}$ value estimated from the CO mapping (0.15–1.2 $L_\odot$ Codella et al. 2001). Since $L_{\rm rad}$ and $L_{\rm kin}$ are expected to be roughly equal if the CO molecular outflow is accelerated at the shock front with momentum conservation (Davis & Eislöffel 1995), the difference in these two values may indicate that the outflow inclination angle is actually smaller than the 10°–20° assumed for the derivation of $L_{\rm kin}$. We also remark that the ratio $L_{\rm rad}/L_{\rm bol}$ is about 10^{-2}, which is the value expected for Class 0 protostars given the relationship between these two quantities found by Giannini et al. (2001) (see next section).

3.3. Nature of the jets exciting sources

In Fig. 4 we have indicated with crosses the reddest sources in the field (see Sect. 3.4), in order to identify the possible exciting sources of the observed H_2 jets.

With regard to the outflow I associated with jets A and B, Codella et al. (2001) show that the exciting source

has to be identified with a continuum radio source located close to the IRAS position. This object is not associated with any near infrared counterpart at a K magnitude level of 16.3 mag. This is somehow expected, since the IRAS source has a very steep spectrum with a flux dropping from 145 Jy at 60 μm to 0.56 Jy at 12 μm. In fact Wilking et al. (1993), who obtained the photometry from 1.6 to 20 μm of the sources located around the IRAS position, find one object within the IRAS error ellipse detected only longward to 3.5 μm.

Given the highly embedded nature of the IRAS counterpart, it should be extremely young. An estimate of its age can be given by assuming it equal to the dynamical age of its outflow. The clump B lies at about 0.45 pc from the IRAS source. Assuming a jet velocity of $\sim$40 km s^{-1}, the implied dynamical time is $\sim 8.5 \times 10^4$ yrs; allowing for an outflow inclination of up to 20° (Codella et al. 2001), this time drops to $\sim 3 \times 10^4$ yrs. For the closer knot (A) $t_{\rm d}$ is about only 10^4 yrs. Ages from 10^4 yrs to 10^5 yrs are typical of Class 0 sources (André et al. 2000). To check for the real membership to this class, we have taken the submillimeter fluxes observed in this source from Saraceno et al. (1996) and estimated the ratio $L_{\rm smm}/L_{\rm bol}$, where $L_{\rm smm}$ is the luminosity emitted longward of 350 μm. In Class 0 sources this ratio must be larger than 5×10^{-3}, a value which implies that the envelope mass is $\gtrsim$ than the stellar mass (André et al. 2000). For IRAS 21391 this ratio is 4.6×10^{-2} for $L_{\rm bol} = 350\ L_\odot$, ensuring that this object is a "true" Class 0 source. It is significant that very few Class 0 of luminosity as high as IRAS 21391 have been so far observed (see, e.g., the list in André et al. 2000). The fact to observe one of such high luminosity objects associated with the IC 1396-N globule may be an indication in favour of the suggestion by Sugitani et al. (1991) that star formation by radiative implosion has a greater efficiency in the production of intermediate-mass stars.

Codella et al. (2001) identify the exciting star of outflow III in a millimeter source located at the geometrical center of the outflow. Two infrared sources are present close to this millimeter peak (labelled as (a) and (b) in Fig. 4) both of them with red colors ($H-K \sim 2$, $J-H > 2.8$) and similar K magnitude (13.6 and 13.2 mag). Given their similar near IR magnitudes and distance from the millimeter source, we cannot uniquely distinguish which of the two is the outflow driving source, although source (b) is preferred given its exact location on the symmetric axis of the flow. A bolometric luminosity of about 10 $L_\odot$ is estimated for this source from the millimeter continuum data (Codella et al. 2001).

As regards the other flow (outflow II), a careful inspection of the K image does not allow to identify a possible candidate for the exciting source. No sources are indeed located at the center of the flows or on the outflow axis. This may suggest that these knots are excited by a very embedded object. Assuming the same velocity as the outflow I, outflow II seems to have dynamical timescales of about 2×10^4 yrs, pointing also in this case to the presence of a young protostar.

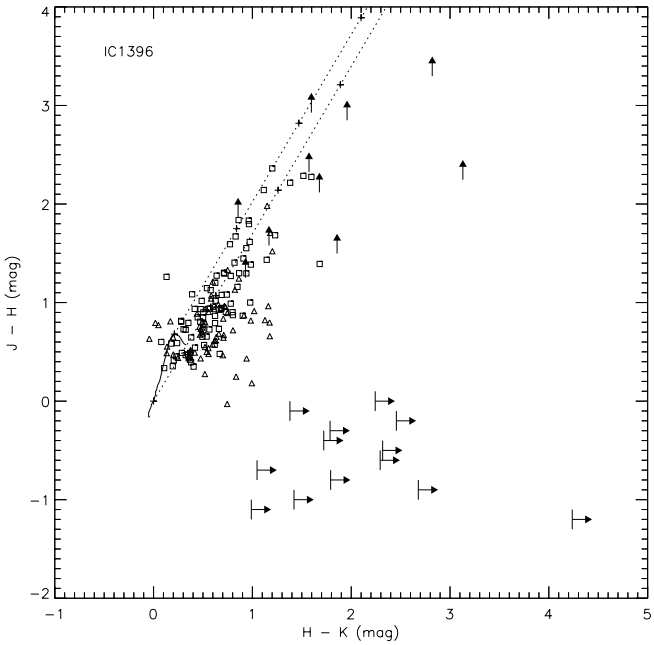

Fig. 6. Color-color diagram of the stars in $4'.4 \times 4'.4$ centered on the IRAS source. The location of the main sequence stars is indicated with a solid line while the two dashed lines are parallel to the reddening vector with crosses at intervals of $A_{\rm V} = 10$ mag. Open squares indicate sources with valid detections in all three bands (open triangles mark sources with K magnitude larger than the completeness limit of 15 mag). Upper arrows indicate sources with un upper limit in the J band, while small vertical segments with rightward arrows indicate sources with a valid detection only in the K band; for these latter, a random $J-H$ color has been assigned to position them on the diagram.

3.4. Young stellar population in IC 1396-N

In Fig. 6, the $J-H$, $H-K$ color-color diagram for the sources in the field centred on the IRAS position is shown. The solid curve is the locus of the unreddened main sequence stars, while the two dashed lines are parallel to the reddening vector and define the band of the reddened normal stellar photosphere. On the right of this band are young sources with intrinsic infrared excesses. In this figure, open squares indicate sources with valid detections in all three bands, upper arrows indicate sources with un upper limit in the J band, while small vertical segments with rightward arrows indicate sources with a valid detection only in the K band; for these latter, a random $J-H$ color have been assigned to position them on the diagram. From the figure it appears that a large fraction of sources are located outside the reddening band, testifying the presence of an embedded young cluster associated with the cloud; this is also evidenced by the averaged large ($\gtrsim$10 mag) extinction inferred from the diagram.

Following Lada & Adams (1992), young stars with colors in a box of about 0.5 mag centred on $J-H$, $H-K \sim 1$ belong to pre-main sequence Classical T Tauri (CTT) stars, while sources with redder colors are less evolved

Table 2. Near IR photometry (in magnitudes) of the embedded young objects in IC 1396-N.

#	α (1950)	δ (1950)	$K(\Delta)$	$H-K(\Delta)$	$J-H(\Delta)$	Notes[1]
1	21:39:06.9	58:03:57	15.808(0.123)	>1.792	...	
2	21:39:07.5	58:02:29	15.143(0.162)	>2.457	...	
3	21:39:07.7	58:04:52	13.188 (0.048)	2.032 (0.08)	>3.18	source (b)
4	21:39:08.2	58:03:05	15.878(0.149)	>1.722	...	
5	21:39:08.2	58:04:44	13.592(0.041)	1.958 (0.080)	>2.850	source (a)
6	21:39:08.8	58:03:12	13.875(0.054)	1.597 (0.082)	>2.928	
7	21:39:08.8	58:02:31	13.023(0.083)	3.130 (0.131)	>2.247	IRS2 of W93
8	21:39:09.2	58:02:57	12.283(0.059)	2.820 (0.089)	>3.297	
9	21:39:11.2	58:03:36	15.307(0.110)	>2.293	...	
10	21:39:11.5	58:02:38	13.363(0.066)	>4.237	...	IRS3 of W93
11	21:39:12.7	58:02:25	12.773(0.038)	1.597 (0.054)	2.275 (0.109)	IRS4 of W93
12	21:39:13.5	58:02:46	14.608(0.155)	1.678 (0.183)	>2.118	
13	21:39:13.8	58:02:00	15.357(0.143)	>2.243	...	
14	21:39:15.1	58:02:01	15.045(0.086)	1.857 (0.197)	>1.498	
15	21:39:15.2	58:03:20	15.282(0.136)	>2.318	...	
16	21:39:15.2	58:02:57	14.502(0.057)	1.573 (0.097)	>2.325	IRS5 of W93
17	21:39:16.5	58:02:20	11.716 (0.023)	1.516 (0.030)	2.286(0.037)	IRS6 of W93
18	21:39:23.0	58:02:51	15.814(0.144)	>1.786	...	
19	21:39:25.1	58:03:01	14.381(0.124)	1.681 (0.151)	1.392 (0.143)	
20	21:38:55.9	58:02:57	14.921(0.118)	>2.679	...	

[1] W93 = Wilking et al. (1993).

Class I type objects. In Table 2, we report the position and the magnitudes of the reddest sources in the field, ($J-H$, $H-K \gtrsim 1.5$ mag) believed to be the youngest of the cluster. Some of these sources were already discovered by Wilking et al. (1993) and are indicated in the table. From this table and from Fig. 4, where the spatial position of these sources is indicated by crosses on the H_2 image of the region, we can see that they form a cluster around the IRAS source position, while some of them (including sources (a) and (b), which are associated with the northen outflow) are also located further north of the cloud rim.

Sugitani et al. (1989) suggested that star formation inside bright rimmed globules is induced by the propagation of the H II ionisation front with the consequent compression due to the radiation pressure. In support to this hypothesis Sugitani et al. (1995) noticed that in different globules in which near IR photometry has been performed, there is a tendency for the young stars to be preferentially distributed along the symmetric axis of the globule towards the direction of the external exciting star; moreover the older stars appear located very close to the bright rim while the redder sources are situated close to the IRAS source which usually appears as the youngest star of the cluster. This distribution suggests a propagation of the star formation from the rim to the interior of the globule as the result of the advancing perturbation induced by the ionisation front.

If we look at the distribution of the young sources in IC 1396-N, we can notice that the young star population is mainly located along a south-north line roughly following the symmetric axis of the globule as found by Sugitani et al. (1995) in similar clouds. We also remark that the young stars appear to cluster along the density distribution inside the globule as evidenced by the CS 3-2 map by Codella et al. (2001). However there is not a clear evidence for an age distribution going from the rim to the globule interior and it is therefore difficult to conclude that the present star formation activity is induced by the ionisation front just on the basis of the source distribution.

4. Conclusions

H_2 narrow band imaging of the IC 1396-N globule reveals the presence of several H_2 jets inside the optically dark region. Such jets are closely associated with CO peaks of high velocity gas. The intrinsic H_2 luminosity of these emission knots is high ($0.1-2.3\ L_\odot$) compared with typical luminosities observed in H_2 jets from young stars (Davis & Eislöffel 1995), indicating that they trace particularly energetic mass ejections. From an analysis of the total radiated shock luminosity in each knot, we estimate that the observed H_2 emission originates from non-dissociative shocks with velocities from 25 to 40 km s^{-1}. The short dynamical time exhibited by the jets ($<5 \times 10^4$ yrs) and the confirmed membership of the IRAS source to the poor evolved Class 0 protostars indicate that the H_2 emission is associated with the most embedded and youngest objects of the field. The near infrared photometry confirms the existence of a cluster of young embedded sources, located along the south-north direction and following the distribution of the high density gas, thus testifying for a highly efficent star formation activity. The present

observations do not however present clear evidences in favour of a triggered mechanism due to the ionisation front.

Acknowledgements. We thanks the referee for her/his valuable comments on the first version of this paper.

References

André, P., Ward-Thompson, D., & Barsony, M. 2000, in Protostar and Planets IV, ed. V. Mannings, A. P. Boss, & S. S. Russell

Barsony, M., Ward-Thompson, D., André, P., & O'Linger, J. 1998, ApJ, 509, 733

Burton, M. G., Hollenbach, D. J., & Tielens, A. G. G. M. 1992, ApJ, 399, 563

Chandler, C. J., & Carlsrom, J. E. 1996, ApJ, 466, 338

Codella, C., Bachiller, R., Nisini, B., Saraceno, P., & Testi, L. 2001, A&A, 376, 271

D'Alessio, F., et al. 2000, Proc. of the SPIE Symp. on Astronomical Telescopes and Instrumentation, ed. M. Iye, & A. F. M. Moorwood, 4008, 748

Davis, C., & Eislöffel, J. 1995, A&A, 300, 851

Elias, J. H., Frogel, J. A., Matthews, K., & Neugebauer, G. 1982, AJ, 87, 1029

Foster, P. N., & Boss, A. P. 1996, ApJ, 468, 784

Giannini, T., Nisini, B., & Lorenzetti, D. 2001, ApJ, in press

Habing, H. J. 1968, Bull. Astr. Inst. Netherlands 19, 421

Hodapp, K. W. 1987, ApJ, 319, 842

Hollenbach, D., Takahashi, T., & Tielens, A. G. G. M. 1991, ApJ, 377, 192

Hunt et al. 1998, AJ, 115, 2594

Kaufman, M. J., & Neufeld, D. A. 1996, ApJ, 456, 250.

Lada, C. J., & Adams, F. C. 1992, ApJ, 393, 278

Masson, C. R., & Chernin, L. M. 1993, ApJ, 414, 230

Nisini, B., Giannini, T., Molinari, S., et al. 1998, in Star Formation with the Infrared Space Observatory, ed. J. L. Yun, & R. Liseau, ASP Conf. Ser., 132, 256

Osterbrock, D. E. 1957, ApJ, 125, 622

Raga, A., & Cabrit, S. 1993, A&A, 278, 267

Saraceno, P., Ceccarelli, C., Clegg, P. E., et al. 1996, A&A, 315, L293

Serabyn, E., Güsten, R., & Mundy, L. 1993, ApJ, 404, 247

Sugitani, K., Fukui, Y., Mizuno, A., & Ohashi, N. 1989, ApJ, 342, L87

Sugitani, K., Fukui, Y., & Ogura, K. 1991, ApJSS, 77, 59

Sugitani, K., Tamura, M., & Ogura, K. 1995, ApJ, 455, L39

Sugitani, K., Matsuo, H., Nakano, M., Tamura, M., & Ogura, K. 2000, ApJ, 119, 323

Wilking, B., Mundy, L., Mc Mullin, J., Hezel, T., & Keene, J. 1993, AJ, 106, 250